Journal of Materials Chemistry B

Accepted Manuscript

ROYAL SOCIETY OF CHEMISTRY

www.rsc.org/materialsB

Integrated 3D Conducting Polymer-based Bioelectronics for Capture and Release of Circulating Tumor Cells

Yu-Sheng Hsiao,* Bo-Cheng Ho, Hong-Xin Yan, Chiung-Wen Kuo, Di-Yen Chueh, Hsiao-hua Yu and Peilin Chen*

Mr. B.-C. Ho, Mr. H.-X. Yan, Prof. Y.-S. Hsiao
Department of Materials Engineering, Ming Chi University of Technology
84 Gunjuan Road, Taishan, New Taipei City 243 (Taiwan)
Fax: (+886)2908-4091
Email: yshsiao@mail.mcut.edu.tw

Dr. H.-h. Yu
Institute of Chemistry
Academia Sinica, Taipei 11529 (Taiwan)

Dr. C.-W. Kuo, Mr. D.-Y. Chueh and Dr. P. Chen
Research Center for Applied Sciences
Academia Sinica, Taipei 11529 (Taiwan)
Fax: (+886)2782-6680
Email: peilin@gate.sinica.edu.tw

Abstract

Here we develop a novel fabrication approach for producing three-dimensional (3D) conducting polymer-based bioelectronic interfaces (BEIs) that can be integrated on electronic devices for rare circulating tumor cell (CTC) isolation, detection, and collection *via* an electrically triggered cell released from chips. Based on the chemical oxidative polymerization of carboxylic acid–modified 3,4-ethylenedioxythiophene and modified poly(dimethylsiloxane) (PDMS) transfer printing technology, the high-aspect-ratio structures of poly(3,4-ethylenedioxythiophene) (PEDOT)-based "nanorod" arrays can be fabricated on indium tin oxide (ITO) electrodes when using the Si "microrod" arrays as masters. Furthermore, we integrated the biotinylated poly-(L)-lysine-*graft*-poly-ethylene-glycol (PLL-*g*-PEG-biotin) coating with 3D PEDOT-based BEIs for dynamic control of the capture/release performance of CTCs on chips; this combination exhibited an optimal cell-capture yield cells of ~ 45000 cells cm^{-2} from EpCAM-positive MCF7 while maintaining resistance from the adhesion of EpCAM-negative Hela cells at a density of ~4000 cells cm^{-2}. By taking advantage of electrochemical doping/dedoping properties of PEDOT materials, the captured CTCs can be triggered to electrically release through the desorption phenomena of PLL-*g*-PEG-biotin. More than 90% of the captured cells can be released while maintaining very high cell viability. Therefore, it is conceivable that use of a 3D PEDOT-based BEI platform will meet the requirements for the development of downstream characterization of CTCs, as well as the next generation of bioelectronics for biomedical applications.

Keywords: Poly(3,4-ethylenedioxythiophene) (PEDOT) • Bioelectronic Interfaces (BEIs) • Circulating Tumor Cell (CTC) • epithelial cell adhesion molecule (EpCAM) • Nanostructured Materials.

Introduction

Bioelectronics is gaining ground in biomedical applications where bioelectronic devices can offer electrical signals for monitoring biological activities, [1-3] electrical stimulation (ES) for medical treatments, [4-6] and electrically triggered-responses for drug or cell release with closed-loop feedback control. [7-9] To date, there are a variety of bioelectronic devices for interfacing artificial electronic devices with living systems and for real clinical systems. [1, 6, 10-13] Therefore, it is widely known that a new class of medical devices can be implanted in the human body for precisely modulating the electrical signaling patterns of the peripheral nervous system or operating as a non-invasive method for *in vitro* liquid biopsy applications. [14-16] Most of the research activities in bioelectronic devices are enabled by integrating bioelectronic interfaces (BEIs) onto the electrodes and/or electronic devices, which are promising intermediate layers that uniquely utilize both electrons and ions as charge carriers for coupling the flows of charges in dual directions, thereby enhancing the communication between the electronics and the biological systems. From the viewpoint of healthcare applications, BEI relies on the selection of organic π-conjugated materials (e.g., conducting polymers and carbon materials) because organic BEI materials can offer significant advantages in facile chemical modification, low impedance with oxide-free interface in aqueous electrolytes, low temperature processing and mass production and high adjustment features for surfaces, including chemical, optical and mechanical properties, through doping/dedoping processes. [6, 10, 12-13]

One of the emerging bioelectronic device applications is the isolation of circulating tumor cells (CTCs). CTCs are cancer cells that break away from a primary tumor or metastatic site, escape from immunosurveillance, and then circulate in the peripheral blood with the capability of forming distant metastases. Distinct from the conventional approaches in the diagnosis of tumor incidence, recurrence and metastases in patients [e.g., fresh tissue biopsy, positron emission tomography (PET), computed tomography (CT), and magnetic resonance imaging (MRI)], [17] it is conceivable that "liquid biopsy for CTC detection" provides no

radiotherapy side effect and can be carried out routinely in patients at all disease sites. Although the tumor liquid biopsy can be easily used for collecting CTCs, the identification of CTCs in patient blood samples is technically challenging because of the extremely low concentration of CTCs among a large number of hematologic cells (red blood cells and leukocytes). To address this unmet need for rare cell isolation, numerous technologies have been developed using physical (e.g., size, density, electric charges and deformability) and biological properties [e.g., surface conjugation with epithelial cellular adhesion molecule antibody (anti-EpCAM)] at the device interfaces. [17-18] Specifically, the unique concept of "NanoVelcro" cell-affinity substrates, using the synergistic effect of nanomaterials and biological immobilization of CTC markers, have been established for enhancing CTC capture efficiency during a liquid biopsy procedure. [19-25] In addition to the pursuit of high-cell-capture yield and specificity from human blood on chips, further vertical integration for the downstream characterization of CTCs is required for future CTC chips, such as liquid biopsy (e.g., single-CTC genotyping for better understanding underlying disease mechanisms and rapid CTC purification for the primary culture to subculturing), for achieving a variety of clinical applications. [25-28]

Recently, electrically conducting polymers [ECPs; e.g., polypyrrole or poly(3,4-ethylenedioxythiophene) (PEDOT)] have been most widely applied to organic BEIs for their outstanding electrical transport and electrochemical charge-discharge properties, inherent biocompatibility, and high manufacturing flexibility. [29-37] When introducing both biochemical and topographical cues to cells, various cell activities (e.g., adhesion, spreading morphologies, proliferation and differentiation) can be manipulated on three-dimensional (3D) BEIs, thereby extending their effectiveness in cell and tissue regulation, as well as in diagnostic and therapeutic applications on the noninvasive blood biopsies. [38-39] In our previous studies that developed 3D PEDOT-based BEIs, carboxylic acid–grafted PEDOT (PEDOTAc) nanostructures were fabricated by electrochemical and chemical oxidative polymerization methods that then allow for conjugation with anti-EpCAM. Therefore, these 3D BEIs can be used as the NanoVelcro cell-affinity chips for enhancing CTC capture performance. [38-

39] However, further study on the fabrication of high-aspect-ratio (HAR) 3D BEI features and their functional integration for dynamic control of biological responses within devices are still needed for development of the next generation of bioelectronics for their application in point-of-care cancer diagnostics.

In this work, we report a novel, easy-to-use approach for fabricating highly regular and HAR PEDOT nanorod array film, and integrate the 3D BEIs into the bioelectronics for use in tumor liquid biopsy applications. Combining the chemical oxidative polymerization and a modified poly(dimethylsiloxane) (PDMS) transfer printing technique, the production principles of 3D PEDOT-based "nanorod" arrays are briefly investigated by using the geometric designs of a Si "microrod" array master (**Figures 1**a-h). Furthermore, we integrated the 3D PEDOT-based BEI devices with the PLL-*g*-PEG-biotin coating for studying the capture efficiency of CTCs in terms of both biochemical and topographical effects, and explored their possibilities for dynamically controlling CTC capture/release performance through the cyclic potential of ES.

Experimental Section

Materials and Reagents

PEDOT Film Fabrication and Surface Modification. Iron(III) *para*-toluenesulfonate hexahydrate [Fe(III)TOS] was obtained from Sigma–Aldrich. Carboxyl-functionalized EDOT (EDOTAc) was synthesized according to a procedure found in the literature (S.-C. Luo, E. M. Ali, N. C. Tansil, H. H. Yu, S. Gao, E. A. B. Kantchev, J. Y. Ying, *Langmuir* **2008**, *24*, 8071). Imidazole (IM) was obtained from TCI. PLL(20)-g[3.5]-PEG(2)/PEG(3.4)-biotin(50%) (PLL-*g*-PEG-biotin) and PLL(20)-*g*[3.5]-PEG(2)/FITC (PLL-*g*-PEG-FITC) were obtained from SuSoS. Streptavidin (SA, 1 mg mL^{-1}) was obtained from Invitrogen. Biotinylated anti-human EpCAM/TROP1 antibody (Goat IgG) was obtained from R&D Systems.

Cell Studies. The breast cancer cell line (MCF7) and cervical cancer cell line (HeLa) were purchased from American Type Culture Collection. GlutaMAX-I, Vybrant® DiO cell–labeling solution and DMEM growth medium were obtained from Invitrogen. Fetal bovine serum (FBS) was obtained from Hyclone; Hoechst 33342 and 4-(2-hydroxyethyl)-1-piperazineethanesulfonic acid (HEPES) buffer were obtained from Life Technologies.

Fabrication and Characterization of Silicon Microrod Arrays

The surfaces of the (100)-oriented silicon (Si) wafers were cleaned using the following procedure. The Si wafers were ultrasonicated in acetone and EtOH at room temperature for 10 and 5 min, respectively, to remove contamination from organic grease. The degreased Si substrates were placed in boiling Piranha solution [H_2SO_4/H_2O_2, 4:1 (v/v)] and RCA solution [$NH_3/H_2O_2/H_2O$, 1:1:5 (v/v/v)] for 1 h each and then rinsed several times with deionized water. The clean Si wafers were spin-coated with photoresist (TMHR ip3650, TOK) and then patterned using I-line projection photolithography (FPA-3000i5+ Stepper, Canon). The designed metal masks were applied with 10-μm square array patterns and a period of 20 μm. After photoresist development, the Si microrod arrays were formed through inductively coupled plasma dry etching (ICP; MESC Multiplex, STS). Relevant parameters for the ICP include: power source, 600 W, bias power, 11.5 W, and two working gases per duty cycle (25 sccm of SF_6 for 7 s; 75 sccm of C_4F_8 for 7 s). The positive Si microrod arrays of various heights were obtained by tuning the etching time, cleaning in boiling Piranha solution [H_2SO_4/H_2O_2, 4:1 (v/v)] to remove the remaining photoresist, treatment with 1*H*,1*H*,2*H*,2*H*-perfluorooctyltrichlorosilane (FOTS; Alfa Aesar) as the anti-stiction coating, and then dicing into silicon masters for subsequent negative poly(dimethylsiloxane) (PDMS) replica-molding.

Fabrication of PDMS Replicates

PDMS prepolymer was first prepared by combining the PDMS base and curing agent at a 10:1 (w/w) ratio (Sylgard 184, Dow Corning) and then blending with an electrical mixer. The mixture of PDMS prepolymer was poured onto the Si micro/nanorod array master, and then the pumping and thermal curing processes were performed. The pumping process helped the PDMS prepolymer fill the nanostructures of the Si master in thermal curing conditions of 70 °C for 3 h. Finally, the obtained negative PDMS hole array replicates were ready for the subsequent transfer printing technique.

Poly(3,4-ethylenedioxythiophene) (PEDOT)-based Microrod Arrays

Chemical Oxidative Polymerization of PEDOTAc films. We generated the negative PDMS hole array replicas from the FOTS–coated Si micro/nanorod arrays that were patterned through I-line projection photolithography and ICP reactive ion etching of the exposed Si. By using an Si master featuring a diverse range of designed microrod structures, we could prepare PEDOT-based microrod arrays from the respective precursors through a negative PDMS transfer printing process that was previously described in detail (Y.S. Hsiao, S.C. Luo, S. Hou, B. Zhu, J. Sekine, C.W. Kuo, D.Y. Chueh, H.H. Yu, H.R. Tseng, P. Chen, *Small* **2014**, *10*, 3012). First, solutions of IM (1.47 M; inhibitor) and Fe(III)TOS (2.56 M; oxidizing agent) were prepared in MeOH in separate flasks at 60 °C. The PEDOT precursor was prepared by mixing a separate vial containing the EDOT derivative (67 mg of EDOTAc) with IM solution (1.8 mL) and the Fe(III)TOS solution (1.8 mL). For chemical oxidative polymerization, the mixture was spun (2000 rpm, 10 s) onto air plasma–treated negative PDMS replicas and then placed directly on a hotplate (105 °C) with a covered glass Petri dish. Air plasma treatment (10 mTorr, 30 s) of the PDMS replicates was performed using a plasma cleaner (Harrick Plasma, PDC-32G). After 10 min of polymerization, the coated wet film turned from a yellow solution into a dark-green/blue solid film. In addition, the polymerized film thickness could be increased by repeating the process of spin-coating and polymerization of the PEDOT precursor. This film was cooled to room temperature and washed three times with MeOH to remove excess Fe(III)TOS and unreacted EDOTAc monomers. Consequently, a demolding step with a glycerol layer was used as an adhesive layer between the PEDOT and 3-aminopropyltrimethoxysilane (APTS)-modified ITO glass substrate, thereby obtaining uniform PEDOTAc/TOS coaxial microrod arrays through PDMS transfer printing techniques.

Device Assembly and Surface Modification on PEDOTAc films. The device assembled from the 3D PEDOTAc-based BEI coated ITO glass consists of a cylindrical PDMS chamber of approximately 4 mm height and 10 mm diameter. The device was treated with PLL-*g*-PEG-biotin [100 μg mL^{-1} in 10 mM HEPES buffer

(pH 7.4)] for 1 h and then incubated with SA (10 μg mL^{-1} in 1× PBS) for 1 h at room temperature. Biotinylated anti-human EpCAM/TROP1 antibody (10 μg mL^{-1} in 1× PBS containing 0.1% BSA and 0.09% NaN_3; 25 μL) was placed onto the device, which was then incubated (60 min) at room temperature. Finally, the 3D PEDOTAc-based BEI devices were washed several times with 1× PBS and then immersed in 1× PBS for 1 h prior to performing the cell experiments.

Scanning Electron Microscopy (SEM)

A scanning electron microscope (FEI Nova NanoSEM 200; accelerating voltage: 10 keV) was used to observe the surface morphologies of the PEDOT-based nanorod arrays and CTCs on chips. Prior to SEM examination, the biological and PEDOT-based samples were dehydrated in ascending grades of EtOH (25, 50, 75, and 100%; each dehydration time: 20 min), subjected to critical point drying with liquid CO_2, and sputter-coated with gold (<3 nm).

Cell Capture/Release Experiments

After removing the 1X PBS from 3D PEDOTAc-based BEI devices, 100 μl cell suspensions (10^5 cells mL^{-1}) were loaded on chips. After incubation for 1 h at 37 °C, 5% CO_2, the substrate was gently washed with 1X PBS (at least five times). Imaging and counting of cells was performed using a fluorescence microscope (CKX41, Olympus). Cell counts for dilution experiments and cell viabilities were conveniently determined using an automated cell counter (Luna™ automated cell counter, Logos Biosystems, Korea). Following the capture procedure described above, substrate-modified cancer cells were trypsinized and collected. Finally, the collected cells on each device were prepared in a 100 μl cell suspension that was then carefully transferred to a counting slide for the Luna™ Automated Cell Counter apparatus. Cell viability was analyzed in triplicate. For the electrically triggered cell-releasing studies, the 3D PEDOTAc-based BEI devices were operated with a standard three-electrode setup consisting of a counter electrode (C.E., Pt), a reference electrode (R.E., Ag/AgCl), a working electrode (PEDOTAc-based nanorod arrays coated ITO glass), and cyclic potential electrical

stimulation (ES) with the voltage swept from –0.8 to +0.5 V at a scan rate of 100 mV s^{-1} for *20* cycles in 1× PBS. All the experiments were repeated more than three times and showed similar results. A confocal microscope (FV1000; Olympus) was used to observe fluorescence images of PLL-*g*-PEG-FITC monolayers on 3D PEDOT-based BEI devices, as well as to monitor the changes in fluorescence density after ES.

Results and Discussion

Using the basis of our previously developed 3D PEDOT-based BEI concepts for CTC isolation, [39] we have demonstrated that the optimized surface biochemical and dimensional controls of 3D PEDOT-based nanorod arrays would provide efficient cell-substrate interaction between the structures of the cellular surface components (e.g., microvilli) and the underlying substrates, thereby increasing the CTC capture performance. However, the device design, using the low aspect-ratio (AR) of PEDOT-based nanorod arrays and a demolding step using a non-conducting UV-curable adhesive, would hinder its bioelectronic applications because of its low integration level between artificial devices and living systems. As shown in **figure** 1, we propose a modified method for fabricating various ARs of PEDOT-based nanorod arrays on the ITO glass; it can be performed readily with precise control of chemical oxidative polymerization and PDMS transfer printing technique. Interestingly, different geometric designs of Si "microrod" array masters can be further used for obtaining different PEDOT-based "nanorod" arrays with high aspect-ratio (HAR) on-chips. Briefly, the production principles and manufacturing processes are described as follows in steps (1-4):

Step (1): a positive Si master featuring a desired microrod dimension was used to obtain negative PDMS hole array replicates for the subsequent transfer printing technique (**Figures** 1a-c).

Step (2): the PEDOTAc precursor, containing EDOTAc monomers with both iron (III) tosylate (as oxidizing agent) and imidazole (as inhibitor), filled the air plasma treated-PDMS hole arrays by using a spin-coating method (**Figure** 1d). Then, the wet PEDOTAc precursor film prepared on the PDMS stamp underwent slow polymerization at 105 °C for 10 min in a covered glass Petri dish (**Figure 1**e).

Step (3): the PEDOTAc film was cooled to room temperature and washed three times with MeOH to remove excess Fe(III)TOS and unreacted EDOTAc monomers.

Step (4): a demolding step was achieved by placing the glycerol-coated ITO glass in close contact with the PEDOTAc layer-coated PDMS replicate and heated at 130 °C for 15 min (**Figures 1**f-g). Wet glycerol thin film can serve as an adhesion/rigidity control agent and can be removed after the baking step, which provides the conformal contact between the polymer layer to be transferred and the hard ITO glass. Finally, a MeOH washing procedure with thermal treatment at 130 °C for 1 h is needed to remove all the glycerol residues from 3D PEDOTAc-based BEIs.

Figure 1h (upper panel) displays an SEM image of 3D PEDOTAc-based rod arrays, where the distribution of rod sizes is very broad, that were directly transferred to the ITO glass without any MeOH washing procedure. It is evident that the left side of the rod was approximately 2 μm in width, equal to the size of the designed Si microrod arrays, whereas the right side of the two rods exhibited a unique core-shell structure. It is very likely that the one-step chemical oxidative polymerization on the negative PDMS replicate gave rise to formation of PEDOTAc/TOS coaxial microrod arrays, which revealed that the geometrical features are composed of a PEDOTAc-based nanorod core that is surrounded by a thick TOS layer. To confirm our hypothesis, TOS coatings were removed from the PEDOTAc/TOS coaxial microrod arrays by washing with MeOH three times to obtain PEDOTAc-based nanorod arrays (**Figures 2**a-d). Although the growth mechanism of PEDOTAc/TOS coaxial microrod arrays is not completely understood, the preferential formation of PEDOTAc-based nanorod arrays may be derived from the phase segregation of EDOTAc and TOS materials during the polymerization process on PDMS replicates (**Figure 1**i).

After using a large amount of MeOH to wash away all the non-reacted residues, various ARs of free-standing PEDOTAc-based nanorod arrays without a TOS shell can be obtained as shown in **figures 2**a-d. **Table 1** reveals that positive Si masters (**Si-*X***) featuring microstructural (width: 2 μm; height: 2, 4, 6, 8, or 10 μm;

period: 4 μm) designs allowed us to efficiently produce PEDOT-based nanorod arrays (width: 0.5-0.77 μm; height: 0.9, 1.78, 2.3, 2.5 or 3.7 μm; period: 4 μm) in comparison with a flat structure; however, the replication fidelity of nanostructures would decrease to 82% by using the 10 μm-height of Si masters. To show that our PEDOTAc:TOS nanorod arrays can be used for BEI applications, we first examined the electrical properties on PEDOTAc-based devices (**P-*X***), where ***X*** refers to a PEDOTAc film that is flat or has a designed microstructure of Si masters. For example, the nanorod arrays of **P-*8*** are fabricated by using the microrod arrays of **Si-*8*** (**Figures 3**a-b). Because the replication fidelity of PEDOTAc nanorods fabricated with the **Si-*10*** master was not 100%, the **P-*10*** device was not used in testing the electrical properties and the CTC capture performance (**Figure 2**d). As shown in **figure 2**e, the proposed 3D PEDOTAc-based BEI device consists of two components: a PDMS well and the 3D PEDOTAc-based BEI coated ITO electrode. The cyclic voltammetry (CV), electrochemical impedance spectrum (EIS) and electrically triggered cell-releasing results were carried out using the standard three-electrode system with 3D PEDOTAc-based BEI devices.

First, CV (voltage swept from –0.8 to 0.5 V) was used to explore the charge capacity density (CCD) of PEDOTAc BEIs with various dimensions in phosphate-buffered saline (PBS, 0.1 M, pH 7.2) (**Figure 3**a). The higher CCD of **P-*8*** (9.18 mC cm^{-2}) indicates that its features had a higher surface area than other structures (**P-*FLT***, **P-*4***, **P-*6***; 4.28 mC cm^{-2}, 7.44 mC cm^{-2}, 8.68 mC cm^{-2}, respectively) and were capable of more-efficient reduced (dark sky-blue) and oxidized (light grey-blue) states for releasing cells (**Figures 3**c-d) relative to that of the ITO electrode (0.21 mC cm^{-2}). In addition, we used EIS to measure the impedance of the devices in the frequency range from 1 to 10^5 Hz (**Figure 3**b). The impedance of PEDOTAc materials at 1 Hz was approximately two orders of magnitude lower than that of the bare ITO electrodes in PBS (0.1 M, pH 7.2), indicating that the PEDOTAc-based BEI would readily undergo ionic exchange, as well as the doping/dedoping process, during the cyclic potential of ES. As mentioned in previous reports, [7, 12, 32] the electrochemical polarization of substrates would result in a local pH change, which led to dissolution of the PLL-*g*-PEG

monolayer from electrodes, allowing for cell sheet recovery and neurite extension in neurons. Therefore, we expected an integrated 3D PEDOTAc-based BEI device with the PLL-*g*-PEG-biotin to exhibit efficient performance for the capture and electrically triggered cell release of CTCs.

The key concept for the capture/release of CTCs is the dynamic control of PLL-*g*-PEG-biotin coating on the 3D PEDOT-based BEI devices. To prove the concept of on-chip manipulations for CTCs, the FITC-PLL-*g*-PEG was first coated onto the surface of the PEDOTAc-based nanorod arrays, and then 20 cycles of CV sweeping (voltage swept from –0.8 to 0.5 V) was used as the electrical stimulation (ES) for electrically triggered diminishing of fluorescence intensity (**Figure 4**a). **Figures 4**b-c shows that one hour after soaking in the FITC-PLL-*g*-PEG solution (100 μg mL^{-1} in a 10 mM HEPES buffer), the **P-*8*** devices would reach saturated adsorption; the nanorod structures were surrounded by a uniform fluorescence coating. According to the previous reports on ES for electrically triggered drug/cell release, [7-9, 15] negligible disruptions were observed in cell function and viability even when using the potential ranges from –1 to 1 V. Therefore, it is believed that hole transportation driven by oxidation of the PEDOTAc backbone would not only result in the desorption of FITC-PLL-*g*-PEG from the PEDOTAc surface but also ensure cell viability and biological functions for the downstream characterization of CTCs.

To demonstrate the potential use of 3D PEDOT-based BEI devices as the liquid biopsy method for personalized cancer diagnostics, we first examined the size- and chemical-dependent cell capture on devices (**P-*FLT***, **P-*2***, **P-*4***, **P-*6***, and **P-*8***); the device configuration was based on a sequence of surface modification processes using PLL-*g*-PEG-biotin, streptavidin (SA), and biotinylated anti-EpCAM (**Figure 5**). The PLL-*g*-PEG-biotin monolayers interacted with the negative charge of PEDOTAc surfaces by electrostatic attraction; then, the high-affinity SA would link the biotinylated anti-EpCAM to the PLL-*g*-PEG-biotin monolayers on the devices, thereby providing the specific binding for CTCs. Because our previous studies showed that the maximum cell-capture numbers were achieved at an incubation time of 50 min, we individually incubated the

MCF7 breast cancer cells (EpCAM-positive cell line) and HeLa cervical cancer cells (EpCAM-negative cell line) on devices for 1 h. Due to the specific cell-substrate interactions on our devices and their high degrees of transparency, we used an inverted optical microscope to monitor the cell-capture efficiency by using the bright-field phase-contrast images of cells captured on chips (**Figure 6**a). Accordingly, the extremely higher cell-capture yields of MCF7 cells and lower nonspecific background of HeLa cells are consistently observed with the NanoVelcro concept for CTCs [38-39]. The results of cell-capture efficiency are summarized in **figure 5**g; the MCF7 cell-capture density did experience a size effect, exhibited in the range of 25000–45000 cells cm^{-2} and increasing in the following order (**P-*FLT*< P-*2*< P-*4*< P-*6*< P-*8***). Based on the previous report for increasing the specific binding with the PLL-*g*-PEG-biotin biointerface, [40] its integration on our 3D PEDOTAc-based nanorod arrays would provide the optimized PEG density that is sufficient to guarantee both nonspecific HeLa cell binding resistance and a sufficient number of biotins for SA binding. Therefore, it is believed that this PEDOT-based 3D BEI film holds the ability to readily integrate with other biotinylated antibodies, allowing for rapid rare cell isolation.

To validate that our BEI device system has the application possibility for adapting the downstream characterization of CTCs, the optimized **P-*8*** device was selected for demonstrating the effectiveness of dynamic control for the capture/release of CTCs (**Figure 6**). As expected, 20 cycles of CV sweeping (voltage swept from –0.8 to 0.5 V) resulted in approximately 90% of MCF7 cells released from the **P-*8*** device (**Figures 6**a-b). Furthermore, **figures 6**b (inset) and **6**c display the optical and SEM images of the captured MCF7 cells, respectively; the extended pseudopodia of cellular structures and nanorod arrays are well matched to obtain sufficient contact. This is understandable because there were 10% of cells remained attached to the surface when the **P-*8*** device underwent the cyclic potential of ES because of the strong cell adhesive forces between the target MCF7 cell and the device. To further investigate the level of voltage needed for sufficient cell release, we applied 20 cycles of a variety of CV sweeping conditions (voltage swept from –0.8 to 0 V, 0 to 0.5 V, –0.8 to

0.5 V) (**Figures 6**d). These results show that the sweeping voltage in the range from –0.8 to 0.5 V would result in higher cell-release performance than others, which might arise from the higher doping/dedoping level of PEDOTAc surfaces and/or more local pH changes during a cyclic potential ES [7, 9, 12, 32]. With the aim of applying the function of electrically triggered cell release for downstream characterization of CTCs, we first explored the possible use of devices for capture/release of MCF7 cells at a series of low cell densities (spiked 10, 50 and 100 cells in 100 μl cell suspension), which revealed that the cell-capture yield at each different spiked cell density was greater than 90%, and the yield of cells remained on **P-*8*** after ES was less than 15% regardless of the number of cells spiked (**Figures 6**e). Furthermore, we examined the test-retest reliability of devices for three cycles of cell capture/release. By repeatedly conducting a sequence of PLL-*g*-PEG-biotin coatings prior to cell capture/release studies, the cell capture and release performance of the device in new cycles could be restored in approximately 45000 cells cm^{-2} and 5000 cells cm^{-2} of cell density, respectively (**Figures 6**f). Using the van der Waals force to cause self-sticking between adjacent PEDOT nanorods, **figure 7**a presents a SEM image of **P-*8*** recorded after three cycles of ES tests; its geometrical structure features similar PEDOTAc-based nanorod arrays structure before ES. It is evident that repeated ES for cell release would not reduce the cell-capture performance on chips because no geometric changes of PEDOTAc-based nanorod arrays occurred. Furthermore, **figures 7**b-d reveals that our 3D PEDOTAc-based nanorod arrays not only provide as high as approximately 90% of viability for released cells [off-chip cultured on tissue culture polystyrene (TCPS) dishes] but also preserve the viability for expanding cultures (on-chip cultured on **P-*8*** device).

Conclusions

We have demonstrated a universal 3D BEI fabrication process for producing high-quality and large 3D PEDOT-based nanorod array films on ITO electrodes, which can be further integrated with a sequencing coating of PLL-*g*-PEG-Biotin, SA and biotinylated capture agents for dynamic control of CTC capture/release. This organic BEI device system can serve as a liquid biopsy chip and features several advantageous characteristics including: (1) diverse dimensional nanorod arrays (tunable from the low to high aspect ratio) for

fine tuning cell-substrate interactions, (2) easily incorporated different immunoaffinity ligands by SA-biotin interactions for compatible integration with different biological systems, (3) high CCD and low impedance properties for bioelectronic operations, (4) high optical transparency for observation from below with an inverted optical microscope, and (5) high viability of the cell cultured on-chip and off-chip. The **P-*8*** device (with a 700 nm width) not only exhibits optimal cell-capture performance for capturing targeted MCF7 cells and excluding the non-targeted HeLa cells but also preserves the ability to efficiently release CTCs via a cyclic potential ES; it could be used to isolate CTCs with negligible disruption of the CTCs' viability and functions. Therefore, it is conceivable that this PEDOT-based 3D BEI film holds the ability to readily integrate with other technologies that greatly improve the efficiency of CTCs analyses after being captured. For the development of powerful and cost efficient clinical therapeutic intervention platforms for monitoring tumor progression and metathesis, future work will integrate this 3D BEI system with more in-depth studies of cancer staging by impedance monitoring technologies, [16] as well as providing rapid rare cell isolation for CTC genotyping to verify the CTC's role as a tumor liquid biopsy. [28]

Acknowledgments

The research endeavors at Ming Chi University of Technology were supported by the Ministry of Science and Technology (MOST) of Taiwan (contracts NSC 103-2218-E-131-002 and MOST 103-2221-E-131-002-MY2). The study conducted in Academia Sinica was supported in part by the Ministry of Science and Technology (MOST) of Taiwan under contract MOST 103-2113-M-001-008-MY3 and by the Academia Sinica Research Project on Nano Science and Technology and Thematic Project. CWK would like to acknowledge the financial support received from the MOST funding award NSC-102-2113-M-001-019-MY3.

References

1. N. Tandon, C. Cannizzaro, P. H. Chao, R. Maidhof, A. Marsano, H. T. Au, M. Radisic and G. Vunjak-Novakovic, *Nat. Protocols*, 2009, **4**, 155-173.
2. A. P. Alivisatos, A. M. Andrews, E. S. Boyden, M. Chun, G. M. Church, K. Deisseroth, J. P. Donoghue, S. E. Fraser, J. Lippincott-Schwartz, L. L. Looger, S. Masmanidis, P. L. McEuen, A. Nurmikko, H. Park, D. S. Peterka, C. Reid, M. L. Roukes, A. Scherer, M. Schnitzer, T. J. Sejnowski, K. L. Shepard, D. Tsao, G. Turrigiano, P. S. Weiss, C. Xu, R. Yuste and X. Zhuang, *ACS Nano*, 2013, **7**, 1850-1866.
3. K. Birmingham, V. Gradinaru, P. Anikeeva, W. M. Grill, V. Pikov, B. McLaughlin, P. Pasricha, D. Weber, K. Ludwig and K. Famm, *Nat. Rev. Drug Discov.*, 2014, **13**, 399-400.
4. A. L. Benabid, S. Chabardes, J. Mitrofanis and P. Pollak, *Lancet Neurol.*, 2009, **8**, 67-81.
5. M. E. Spira and A. Hai, *Nat. Nanotech.*, 2013, **8**, 83-94.
6. P. Fattahi, G. Yang, G. Kim and M. R. Abidian, *Adv. Mater.*, 2014, **26**, 1846-1885.
7. O. Guillaume-Gentil, Y. Akiyama, M. Schuler, C. Tang, M. Textor, M. Yamato, T. Okano and J. Vörös, *Adv. Mater.*, 2008, **20**, 560-565.
8. K. M. Persson, R. Karlsson, K. Svennersten, S. Loffler, E. W. Jager, A. Richter-Dahlfors, P. Konradsson and M. Berggren, *Adv. Mater.*, 2011, **23**, 4403-4408.
9. Y.-S. Hsiao, C.-W. Kuo and P. Chen, *Adv. Funct. Mater.*, 2013, **23**, 4649-4656.
10. M. Berggren and A. Richter-Dahlfors, *Adv. Mater.*, 2007, **19**, 3201-3213.
11. D. T. Simon, S. Kurup, K. C. Larsson, R. Hori, K. Tybrandt, M. Goiny, E. W. H. Jager, M. Berggren, B. Canlon and A. Richter-Dahlfors, *Nat. Mater.*, 2009, **8**, 742-746.
12. J. Rivnay, R. M. Owens and G. G. Malliaras, *Chem. Mater.*, 2014, **26**, 679-685.
13. G. Lanzani, *Nat. Mater.*, 2014, **13**, 775-776.

14. M. Abdolahad, M. Taghinejad, H. Taghinejad, M. Janmaleki and S. Mohajerzadeh, *Lab Chip*, 2012, **12**, 1183-1190.

15. S. Jeon, J. M. Moon, E. S. Lee, Y. H. Kim and Y. Cho, *Angew. Chem. Int. Ed.*, 2014, **53**, 4597-4602.

16. M. Abdolahad, H. Shashaani, M. Janmaleki and S. Mohajerzadeh, *Biosens. Bioelectron.*, 2014, **59**, 151-159.

17. B. Hong and Y. Zu, *Theranostics*, 2013, **3**, 377-394.

18. R. Harouaka, Z. Kang, S. Y. Zheng and L. Cao, *Pharmacol. Ther.*, 2014, **141**, 209-221.

19. S. Wang, H. Wang, J. Jiao, K. J. Chen, G. E. Owens, K. Kamei, J. Sun, D. J. Sherman, C. P. Behrenbruch, H. Wu and H.-R. Tseng, *Angew. Chem. Int. Ed.*, 2009, **48**, 8970-8973.

20. S. Wang, K. Liu, J. Liu, Z. T. Yu, X. Xu, L. Zhao, T. Lee, E. K. Lee, J. Reiss, Y. K. Lee, L. W. Chung, J. Huang, M. Rettig, D. Seligson, K. N. Duraiswamy, C. K. Shen and H.-R. Tseng, *Angew. Chem. Int. Ed.*, 2011, **50**, 3084-3088.

21. N. Zhang, Y. Deng, Q. Tai, B. Cheng, L. Zhao, Q. Shen, R. He, L. Hong, W. Liu, S. Guo, K. Liu, H.-R. Tseng, B. Xiong and X. Z. Zhao, *Adv. Mater.*, 2012, **24**, 2756-2760.

22. Q. Shen, L. Xu, L. Zhao, D. Wu, Y. Fan, Y. Zhou, W. H. Ouyang, X. Xu, Z. Zhang, M. Song, T. Lee, M. A. Garcia, B. Xiong, S. Hou, H.-R. Tseng and X. Fang, *Adv. Mater.*, 2013, **25**, 2368-2373.

23. S. Hou, L. Zhao, Q. Shen, J. Yu, C. Ng, X. Kong, D. Wu, M. Song, X. Shi, X. Xu, W. H. OuYang, R. He, X. Z. Zhao, T. Lee, F. C. Brunicardi, M. A. Garcia, A. Ribas, R. S. Lo and H.-R. Tseng, *Angew. Chem. Int. Ed.*, 2013, **52**, 3379-3383.

24. L. Wang, W. Asghar, U. Demirci and Y. Wan, *Nano Today*, 2013, **8**, 374-387.

25. M. Lin, J. F. Chen, Y. T. Lu, Y. Zhang, J. Song, S. Hou, Z. Ke and H.-R. Tseng, *Accounts Chem. Res.*, 2014, **47**, 2941-2950.

26. J. G. Lohr, V. A. Adalsteinsson, K. Cibulskis, A. D. Choudhury, M. Rosenberg, P. Cruz-Gordillo, J. M. Francis, C. Z. Zhang, A. K. Shalek, R. Satija, J. J. Trombetta, D. Lu, N. Tallapragada, N. Tahirova, S. Kim, B. Blumenstiel, C. Sougnez, A. Lowe, B. Wong, D. Auclair, E. M. Van Allen, M. Nakabayashi, R. T. Lis, G. S. Lee, T. Li, M. S. Chabot, A. Ly, M. E. Taplin, T. E. Clancy, M. Loda, A. Regev, M. Meyerson, W. C. Hahn, P. W. Kantoff, T. R. Golub, G. Getz, J. S. Boehm and J. C. Love, *Nat. Biotechnol.*, 2014, **32**, 479-484.

27. H. J. Yoon, M. Kozminsky and S. Nagrath, *ACS Nano*, 2014, **8**, 1995-2017.

28. Z. Ke, M. Lin, J.-F. Chen, J.-s. Choi, Y. Zhang, A. Fong, A.-J. Liang, S.-F. Chen, Q. Li, W. Fang, P. Zhang, M. A. Garcia, T. Lee, M. Song, H.-A. Lin, H. Zhao, S.-C. Luo, S. Hou, H.-h. Yu and H.-R. Tseng, *ACS Nano*, 2014, Article ASAP, DOI: 10.1021/nn5056282.

29. M. R. Abidian, J. M. Corey, D. R. Kipke and D. C. Martin, *Small*, 2010, **6**, 421-429.

30. S. Y. Yang, B. N. Kim, A. A. Zakhidov, P. G. Taylor, J. K. Lee, C. K. Ober, M. Lindau and G. G. Malliaras, *Adv. Mater.*, 2011, **23**, H184-188.

31. Y.-S. Hsiao, C.-C. Lin, H.-J. Hsieh, S.-M. Tsai, C.-W. Kuo, C.-W. Chu and P. Chen, *Lab Chip*, 2011, **11**, 3674-3680.

32. C.-H. Lu, Y.-S. Hsiao, C.-W. Kuo and P. Chen, *Biochim. Biophys. Acta*, 2013, **1830**, 4321-4328.

33. L. Jin, T. Wang, Z.-Q. Feng, M. K. Leach, J. Wu, S. Mo and Q. Jiang, *J. Mater. Chem. B*, 2013, **1**, 1818.

34. M. Bongo, O. Winther-Jensen, S. Himmelberger, X. Strakosas, M. Ramuz, A. Hama, E. Stavrinidou, G. G. Malliaras, A. Salleo, B. Winther-Jensen and R. M. Owens, *J. Mater. Chem. B*, 2013, **1**, 3860.

35. Y. Wang, M. Rouabhia and Z. Zhang, *J. Mater. Chem. B*, 2013, **1**, 3789.

36. X. Strakosas, M. Sessolo, A. Hama, J. Rivnay, E. Stavrinidou, G. G. Malliaras and R. M. Owens, *J. Mater. Chem. B*, 2014, **2**, 2537.

37. S. Baek, R. Green, A. Granville, P. Martens and L. Poole-Warren, *J. Mater. Chem. B*, 2013, **1**, 3803.

38. J. Sekine, S.-C. Luo, S. Wang, B. Zhu, H.-R. Tseng and H.-h. Yu, *Adv. Mater.*, 2011, **23**, 4788-4792.

39. Y.-S. Hsiao, S. C. Luo, S. Hou, B. Zhu, J. Sekine, C. W. Kuo, D. Y. Chueh, H. H. Yu, H. R. Tseng and P. Chen, *Small*, 2014, **10**, 3012-3017.

40. L. A. Ruiz-Taylor, T. L. Martin, F. G. Zaugg, K. Witte, P. Indermuhle, S. Nock and P. Wagner, *Proc. Natl. Acad. Sci. USA*, 2001, **98**, 852-857.

Figure Captions

Figure 1. a–g) Schematic representation of the integrated fabrication of a PEDOTAc-based nanorod array on ITO glass. a) I-line projection photolithography on a Si substrate and formation of Si microrod array master after ICP. b) Preparation of PDMS on Si microrod arrays modified with the FOTS vapor. c) Negative PDMS microhole array replicate treated with air plasma (10 mtorr; 30 s). d) PEDOTAc precursor spin-coated on the PDMS replicate. e) Optimized chemical oxidative polymerization of PEDOTAc film in a covered glass Petri dish. f) Wet glycerol film spin-coated on APTS-modified ITO glass substrate. g) Transfer of PEDOTAc/TOS coaxial microrod arrays to the ITO glass with the following MeOH washing procedure. h) Washing away the shell structure of PEDOTAc/TOS coaxial microrod arrays and formation of PEDOTAc-based nanorod arrays; inset: SEM image of PEDOTAc/TOS coaxial microrod arrays during an incomplete washing procedure. i) Schematic representation the polymerization of PEDOTAc precursor with two phase segregation of PEDOTAc and TOS materials on the negative PDMS hole array replicate.

Figure 2. SEM images of PEDOTAc-based nanorod arrays. a–d) **P-*X*** with designed structures (***X***) of a) ***4***, b) ***6***, c) ***8***, d) ***10***. e) Schematic diagram of 3D PEDOTAc-based BEI devices with the PDMS reservoir (Ag/AgCl reference electrode, R.E.; platinum counter electrode, C.E.; PEDOTAc-based nanorod arrays/ITO working electrode, W.E.). (Inset: photograph of a **P-*8*** device for CV, EIS, and capture/release of PLL-*g*-PEG-FITC or CTCs).

Figure 3. Electrical properties of various PEDOTAc-based BEI on ITO glass in 1× PBS. a) CV: Potential swept from –0.8 to 0.5 V at a scan rate of 100 mV s^{-1}. Reduced and oxidized states of PEDOTAc-based BEI were shown at time point A and B, respectively. CCDs for **ITO**, **P-*FLT***, **P-*4***, **P-*6***, and **P-*8*** were 0.21, 4.28, 7.44, 8.68, and 9.18 mC cm^{-2}, respectively. b) Electrochemical impedance spectroscopy (frequency range, 1–10^5 Hz). c–d) Photograph of a **P-*8*** device under cyclic potential ES at c) reduced state and d) oxidized state.

Figure 4. a) Scheme of the mechanism of a PEDOTAc-based nanorod array for electrically triggered PLL-*g*-PEG-FITC release. b) 3D confocal fluorescence image of PLL-*g*-PEG-FITC coated 3D PEDOTAc-based BEI device (**P-*8*** device). c–d) The frequency of a fluorescence signal from the **P-*8*** device was plotted with respect to fluorescence intensity c) without ES and d) with ES.

Figure 5. a–g) Schematic representation of surface modifications for a 3D PEDOTAc-based BEI device and its concept for electrically triggered cell release. a) PEDOTAc-based nanorod arrays. b) PLL-g-PEG-biotin monolayer adsorbed on PEDOTAc-based nanorod arrays. c) PLL-*g*-PEG-biotin is used to form the biotin-streptavidin complex. d) Conjugation of biotinylated anti-EpCAM on devices. e–f) Scheme of the mechanism for capture and release of CTCs on chips, respectively. g) Capture yields of various 3D PEDOTAc-based BEI devices [anti-EpCAM–conjugated **P-*X*** device; ***X*** is the designed structure of Si master] on MCF7 (■) and HeLa (□) cells. MCF7 cells, EpCAM-(+); HeLa cells, EpCAM-(**–**).

Figure 6. a–c) Phase-contrast images of MCF7 cells captured on a **P-*8*** device a) without ES, b) with ES (voltage swept from –0.8 to +0.5 V at a scan rate of 100 mV s^{-1} for *20* cycles in 1× PBS) for cell releasing from the 3D PEDOTAc-based device. Inset: Higher-magnification phase-contrast image of MCF7 cells captured on a **P-*8*** device after ES. c) SEM image of MCF7 cells captured on the **P-*8*** device after ES. d) Quantization of the percentage of MCF7 cells remaining on the surfaces after ES for cell release with a variety of CV sweeping conditions (voltage swept from –0.8 to 0 V, 0 to 0.5 V, –0.8 to 0.5 V) at a scan rate of 100 mV s^{-1} for *20* cycles in 1× PBS. e) Capture efficiency and percentage of cells remained on a **P-*8*** device after ES for spiking 10, 50 and 100 cells in 100 μl of cell suspension. f) Cell capture/release performance of the **P-*8*** device in multiple/sequential rounds of studies with and without ES.

Figure 7. a) SEM image of a 3D PEDOTAc-based BEI device after triple rounds of cell capture/release tests, revealing no geometric changes for the PEDOTAc-based nanorod arrays. b) Cell viability tests for MCF7 cells

captured on the control (TCPS) and **P-*8*** device (w/o ES), and MCF7 cells released from **P-*8*** device (w/ ES). Released cells were washed twice with 1× PBS and incubated for 48 h; error bar represents the standard deviation from three repeats. The viability was assayed through trypan blue exclusion. c) and d) Phase-contrast image of MCF7 cells successfully cultured on-chip (**P-*8*** device) and off-chip (TCPS; cells were released from the **P-*8*** device) after 48 h incubation.

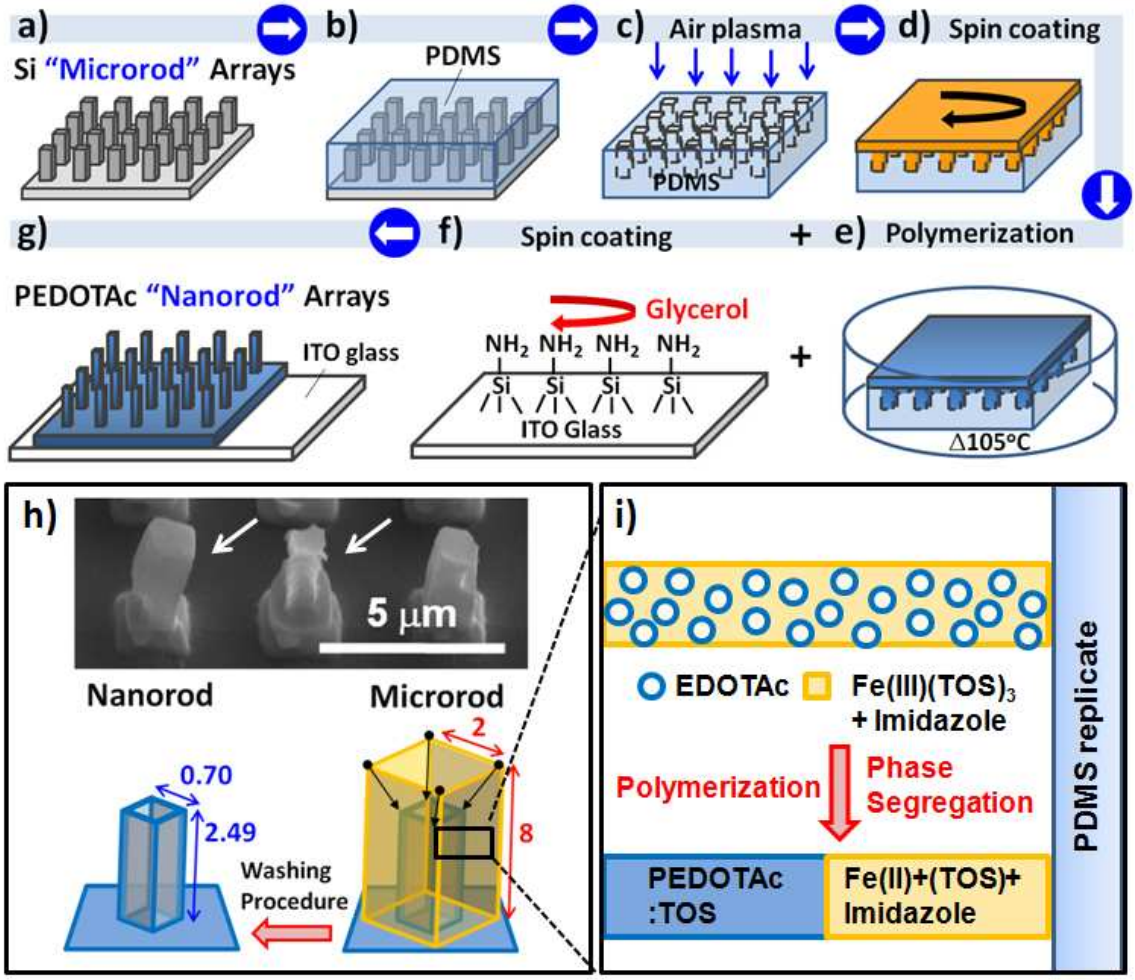

Figure 1

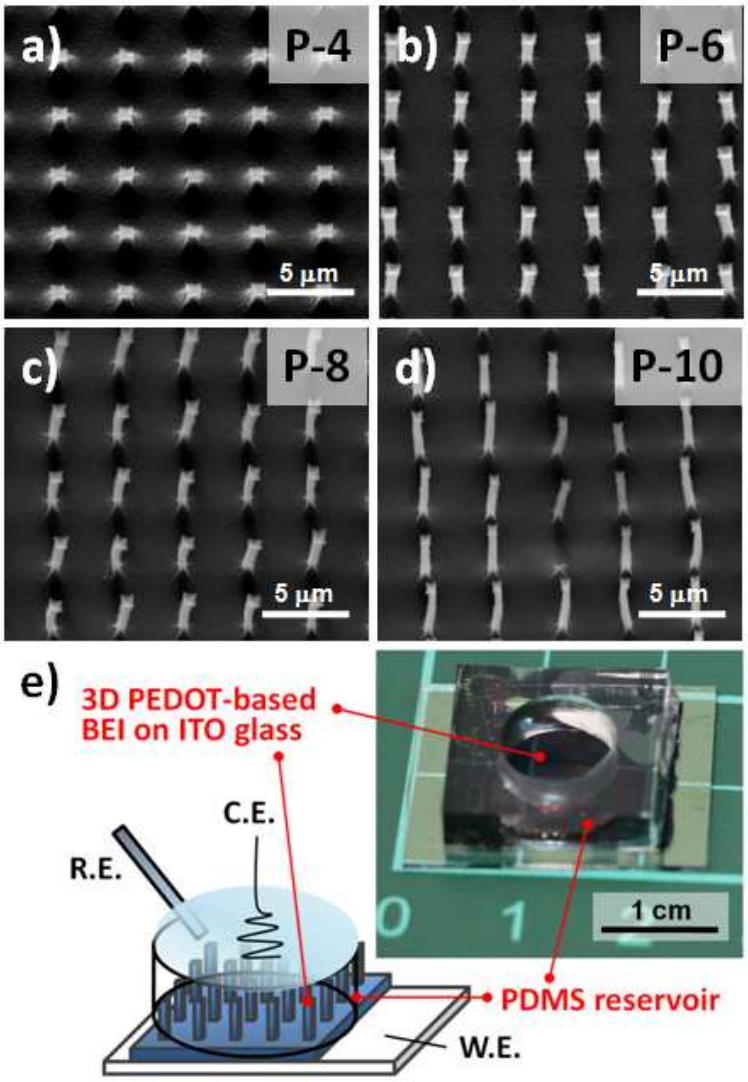

Figure 2

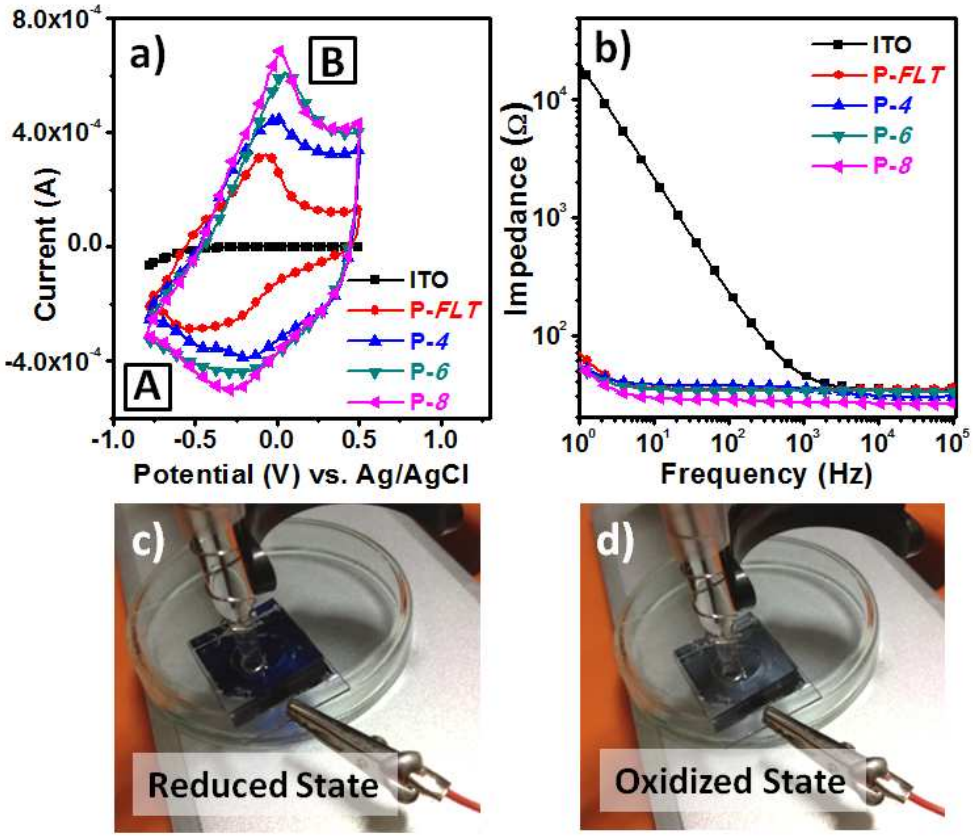

Figure 3

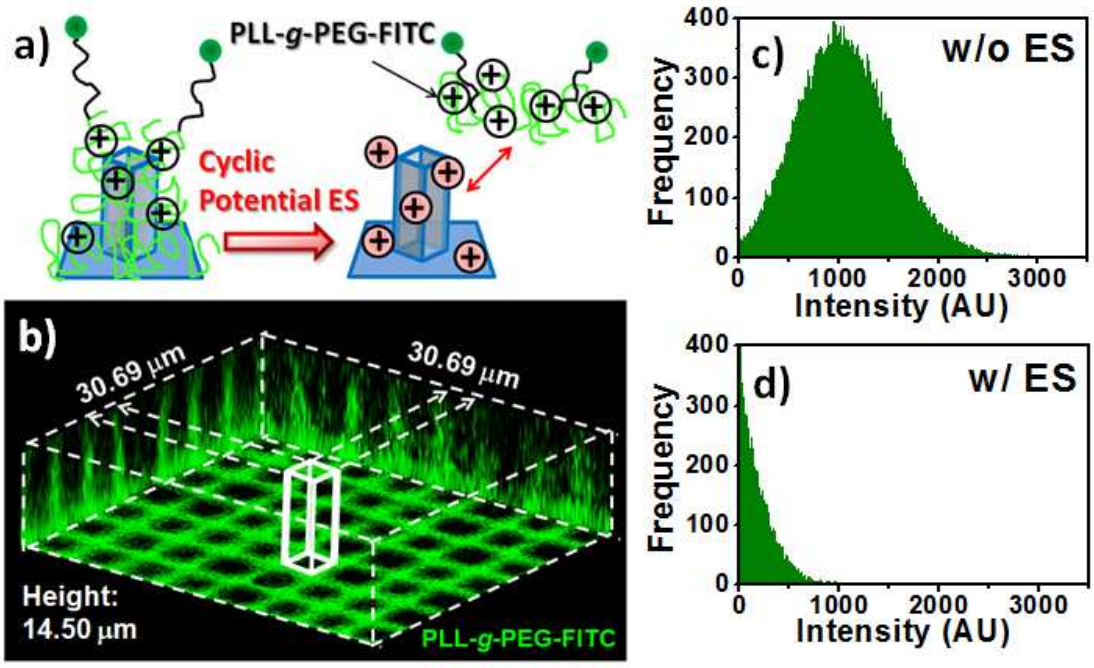

Figure 4

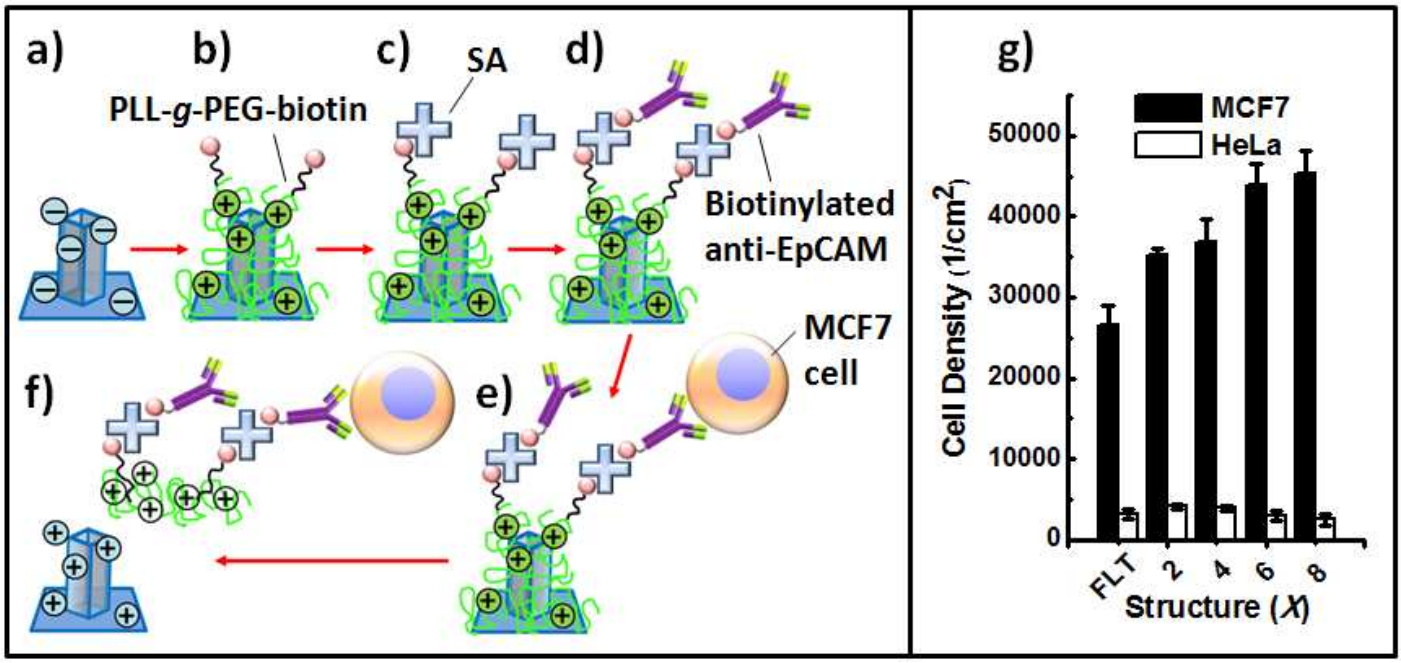

Figure 5

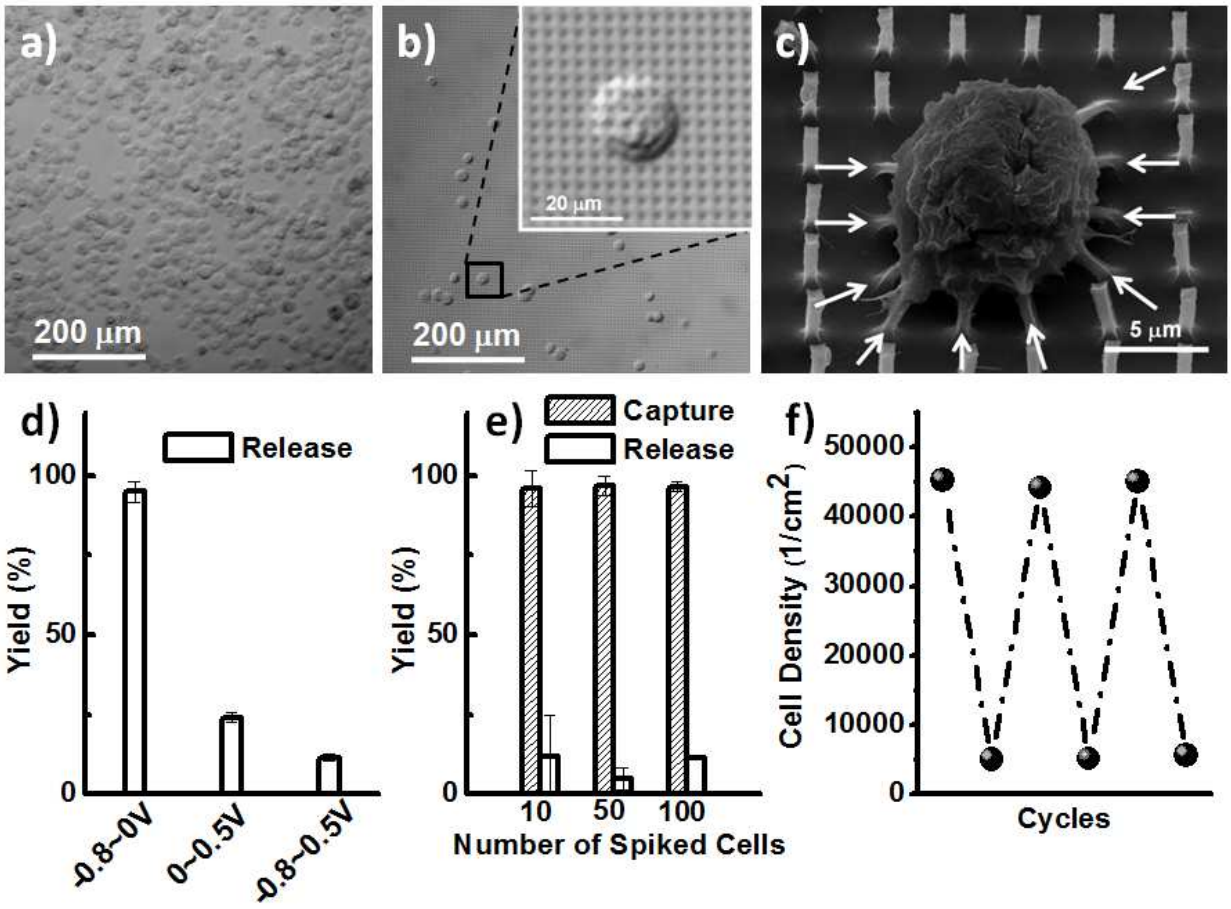

Figure 6

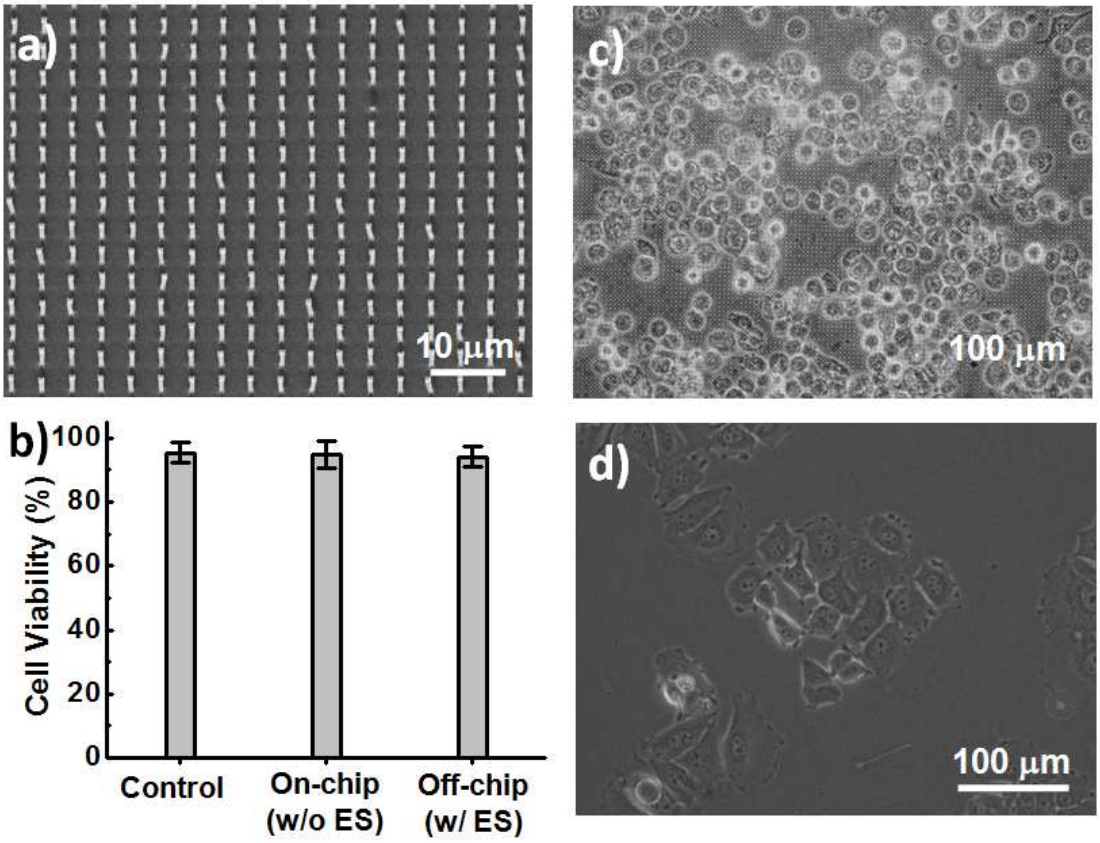

Figure 7

Table captions

Table 1. Geometric parameters of Si microrod array masters and PEDOTAc-based nanorod array devices.

Si microrod arrays[a]					
Master **Si-*X***	Height (*H*; μm)	Width (*W*; μm)	Period (*P*; μm)	Aspect Ratio	Structural Integrity (%)
Si-*2*	2	2	4	1	100
Si-*4*	4	2	4	2	100
Si-*6*	6	2	4	3	100
Si-*8*	8	2	4	4	100
Si-*10*	10	2	4	5	100
PEDOTAc-based nanorod arrays[b]					
Device **Si-*X***	Height (*H*; μm)	Width (*W*; μm)	Period (*P*; μm)	Aspect Ratio	Replication Fidelity (%)
P-*2*	1.02	0.78	4	1.31	100
P-*4*	1.78	0.77	4	2.31	100
P-*6*	2.24	0.70	4	3.20	100
P-*8*	2.49	0.70	4	3.56	100
P-*10*	3.65	0.50	4	7.30	82

a: Values of *W*, *P*, *H* and structural integrity of the Si microrod arrays were identified using SEM.

b: Values of *W*, *P*, *H* and replication fidelity of the PEDOTAc-based nanorod arrays were identified using SEM.

“For Table of Contents Use Only”

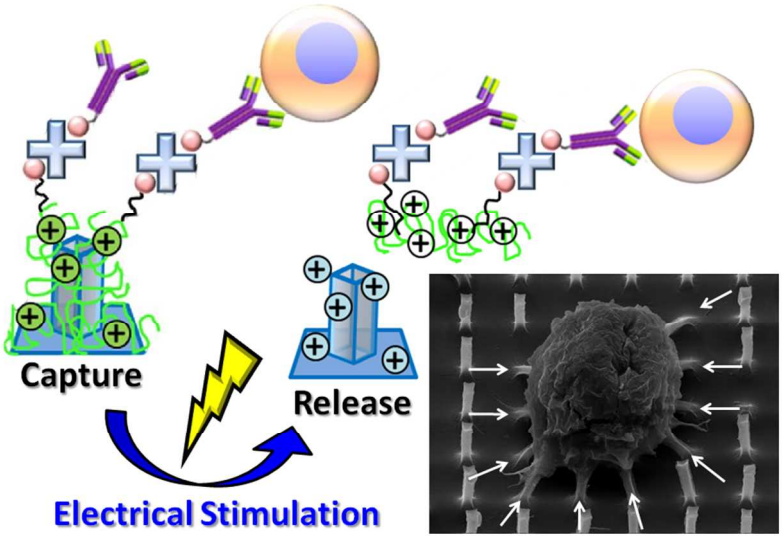

3D conducting polymer-based bioelectronic interface (BEI) devices for dynamically controlling circulating tumor cell capture/release performance through the cyclic potential electrical stimulation.